J Mater Sci: Mater Electron (2026) 37:424

Sodium–lithium co-doping driven enhancement of structure, superconductivity, and vortex pinning in Bi-2212 superconductors

F. Karaçora[1], İ. Ergin[2], M. Gürsul[2], and B. Özçelik[2,*]

[1] *Department of Electrical and Electronic Engineering, Faculty of Engineering, Hakkari University, 30000 Hakkari, Turkey*
[2] *Department of Physics, Faculty of Science and Letters, Çukurova University, 01330 Adana, Turkey*

Received: 21 August 2025
Accepted: 7 February 2026

© The Author(s), 2026

ABSTRACT

This work examines the structural, electrical, and magnetic behaviour of Bi-2212 superconductors co-doped with sodium and lithium, prepared by the conventional solid-state reaction method. Bulk ceramic samples with fixed sodium substitution at the calcium site (y = 0.05) and varying lithium content at the copper site (x = 0.00–0.20) were produced and analysed using X-ray diffraction (XRD), scanning electron microscopy (SEM) coupled with energy dispersive spectroscopy (EDS), DC resistivity, and magnetic techniques. XRD analysis confirmed the dominance of the Bi-2212 phase with minor Bi-2201 and Bi-2223 traces, while Li incorporation promoted the growth of (*00 l*) planes and induced a slight monotonic expansion of the lattice parameters and crystallite size. SEM observations revealed that Na–Li co-doping enhanced grain growth and reduced porosity, leading to improved intergranular connectivity. EDS analysis confirmed the preservation of the Bi-2212 phase composition and revealed a slight decrease in oxygen concentration in Li-doped samples, indicating oxygen deficiency, in agreement with previous reports and the observed c-axis elongation from XRD analysis. Resistivity measurements indicated that optimal doping (Na05–Li10) resulted in the lowest residual resistivity (1.59 mΩ·cm) and the highest superconducting transition temperatures (T_c^{onset} = 85.4 K, T_c^{offset} = 75.28 K). Magnetoresistance data analysed within the thermally activated flux flow (TAFF) framework showed increased vortex activation energies and improved flux pinning with co-doping. Both the irreversibility field $H_{irr}(0)$ and the upper critical field $H_{c2}(0)$ were significantly enhanced, reaching 25.94 T and 48.55 T, respectively, for the Na05–Li10 composition. Magnetic measurements showed enhanced remanent magnetization, increased critical current density (J_c), and stronger flux pinning force, consistent with improved vortex immobilization in the Na–Li co-doped Bi-2212 system. These results indicate that sodium–lithium co-doping significantly enhances the microstructural and superconducting characteristics of Bi-2212, thereby extending its suitability for high-field applications.

Address correspondence to E-mail: ozcelik@cu.edu.tr

https://doi.org/10.1007/s10854-026-16845-5
Published online: 24 February 2026

1 Introduction

Superconductivity, a quantum effect marked by the total loss of electrical resistance and the exclusion of magnetic flux below a critical temperature (T_c), remains a focal point of scientific research because of its vast potential in advanced technological applications. Since the discovery of high-temperature superconductivity (HTS) in the Ba–La–Cu–O system [1], and shortly after in Y-Ba-Cu–O (YBCO) and Bi–Sr–Ca–Cu–O (BSCCO) systems [2, 3], extensive research efforts have been devoted to understanding and improving the physical properties of these materials for practical applications. Among the high-temperature cuprate superconductors, bismuth-based compounds (BSCCO) have attracted significant attention due to their relatively high T_c, chemical tunability, high critical current densities, and strong magnetic field tolerance, making them suitable for practical applications such as fault current limiters, wires and tapes [4–6].

The BSCCO family is typically represented by the formula $Bi_2Sr_2Ca_{n-1}Cu_nO_y$ (n = 1, 2, 3), giving rise to three major phases: Bi-2201 (n = 1, $T_c \approx 20$ K) [7], Bi-2212 (n = 2, $T_c \approx 85$ K) [3], and Bi-2223 (n = 3, $T_c \approx 110$ K) [8]. These phases are distinguished by the number of CuO_2 planes per unit cell, which strongly influence their superconducting and structural properties. The crystal structure of these compounds features a layered arrangement with alternating bismuth oxide, strontium oxide, and copper oxide planes aligned along the c-axis. While the Bi-2223 phase offers the highest T_c, its synthesis is complicated by phase instability, slow reaction kinetics, and difficulty in achieving a single-phase material. The formation of Bi-2223 is often accompanied by residual Bi-2212 intergrowths and requires long sintering times, narrow temperature windows, and controlled atmospheric conditions [9–11]. In contrast, the Bi-2212 phase is more thermodynamically stable and can be synthesized more readily via conventional solid-state methods within shorter durations and broader temperature ranges. These characteristics, along with its lower processing cost and moderately high critical temperature, make Bi-2212 a more practical and scalable candidate than Bi-2223 for technological applications [12]. Nevertheless, its application is limited by drawbacks including weak intergranular links, poor grain alignment, short coherence length, high anisotropy, and sensitivity to applied magnetic fields [13–15]. To overcome these challenges, various fabrication techniques have been investigated, ranging from standard solid-state reactions and polymer-derived methods to sol–gel and co-precipitation processes, as well as more advanced approaches like laser floating zone (LFZ) and electrically assisted laser floating zone growth (EALFZ) [16–21]. The goals of such approaches aim to enhance phase purity, crystallographic alignment, and grain coupling.

An alternative and highly effective method for enhancing the superconducting performance involves element substitution or doping. Through altering carrier concentration, adjusting lattice constants, and creating flux pinning centers, doping enhances the critical current density (J_c) and boosts the material's overall performance [22–26]. Among the various doping strategies, the incorporation of alkali metals (Li^+, Na^+, K^+) has proven particularly effective, owing to their ionic radii being comparable to those of Ca and Cu, as well as their monovalent charge, which enables precise tuning of the hole concentration in the CuO_2 planes and promotes the formation of localized defects that act as flux pinning centers [27–34]. In particular, Li doping has been shown to significantly lower the temperature required for the formation of the Bi-2212 superconducting structure, enabling its development at reduced temperatures. For example, glass-forming Bi-2212 compositions produced by rapid melt-quenching followed by moderate annealing exhibit crystallization into the Bi-2212 phase at temperatures substantially lower than those required for undoped counterparts. This not only accelerates phase formation but also yields T_c values up to 91 K, alongside an increase in the c-axis lattice parameter with rising Li content [35]. Likewise, the T_c enhancement observed in whiskers, attributed to a modified Sr/Ca ratio rather than hole concentration optimization, supports the advantageous role of Li in promoting superconductivity under lower-temperature processing conditions [36]. In addition, Li substitution for Sr or Cu has been shown to enhance the onset and zero-resistance temperatures while reducing the melting point by as much as 140 °C. These effects allow sintering at lower temperatures and support the development of more refined microstructural features [37]. Lithium incorporation at specific lattice sites (e.g., Cu or Ca) also leads to distinct modifications in lattice parameters and superconducting behavior; Li at the Cu site in particular has been correlated with increased T_c and reduced processing requirements [28]. Moreover,

susceptibility and resistivity analyses have demonstrated that lithium improves intergranular connectivity and homogeneity, leading to stronger flux pinning and enhanced overall superconducting performance at optimal doping levels [38].

In addition to lithium, sodium doping has also been demonstrated to significantly enhance the superconducting properties of BSCCO. For instance, melt-processed Na-doped $Bi_2Sr_2CaCu_2O_{8+y}$ samples exhibited an increase in the T_c up to 100 K, which was attributed to an optimal redistribution of hole density in the CuO_2 planes induced by Na incorporation [39]. Electron spin resonance (ESR) studies on Na-doped Bi-2212 polycrystals confirmed that increasing Na concentration at the Ca site raises T_c and decreases the magnetic penetration depth, indicating stronger superconducting coupling and improved vortex lattice properties [40]. Cu *K*-edge X-ray absorption fine structure (XAFS) spectroscopy investigations on $Bi_{1.6}Pb_{0.4}Sr_2Ca_{2-x}Na_xCu_3O_{10+\delta}$ samples revealed that increasing Na content reduces distortions in the CuO_2 planes, leading to a more stable crystal structure. This stabilization is accompanied by a contraction of the in-plane Cu–O bond and an increase in the average Cu valence state, which together contribute to enhanced superconducting behavior [41].

While the individual effects of Na and Li substitution have been extensively studied, their combined (co-doping) influence on the Bi-2212 system has received comparatively less attention.When properly optimized; co-doping strategies can combine the advantages of both elements and provide a broader parameter space for tailoring superconducting performance.

Specifically, Na–Li co-doping may stabilize the hole concentration in the CuO_2 planes, modify the charge distribution, promote the formation of nanoscale pinning centers, and introduce defect structures, all of which collectively contribute to enhancements in transition temperature, critical fields, and current-carrying capacity. In our previous investigations, Na incorporation at the Ca site was shown to significantly improved phase purity, grain connectivity, and key superconducting parameters [23, 31].

Motivated by these findings, the present study seeks to further enhance the superconducting properties of Bi-2212 by partially substituting Ca^{2+} with 5% Na^+ (x = 0.05) and introducing Li^+ substitution at the Cu site. The choice of Cu-site substitution for Li^+ was motivated by previous reports indicating that replacing Cu with Li yields more favorable superconducting characteristics compared to substitution at the Bi, Sr, or Ca sites [27]. Therefore, in addition to fixed Na doping, a series of samples with varying Li content at the Cu site were prepared using the conventional solid-state reaction method, which remains a widely used synthesis route due to its simplicity, scalability, and reproducibility [42, 43]. The synthesized samples were characterized using X-ray diffraction (XRD) to assess phase composition and lattice parameter changes, scanning electron microscopy (SEM) coupled with energy dispersive spectroscopy (EDS) to obtain microstructural and compositional analysis, DC resistivity measurements to probe the field-dependent superconducting transition behavior. To further elucidate the vortex dynamics and the role of flux pinning, magnetoresistance measurements were performed under external magnetic fields ranging from 0 to 5 T. The resulting broadening of the resistive transition was analyzed within the framework of the thermally activated flux flow (TAFF) model [44], allowing extraction of the activation energies (U) as a function of magnetic field.

The variation of these energies with the applied field provides key insights into the efficiency of flux pinning in the Na-Li substituted samples. Additionally, magnetic hysteresis measurements were conducted to determine the remanent magnetization and critical current densities.

In short, this study provides a detailed and systematic examination of how Na–Li co-doping influences the structure, electrical transport, and magnetic characteristics of Bi-2212 superconductors. By correlating these properties with doping level and microstructural evolution, the findings offer valuable insights into the optimization of alkali-doped Bi-2212 systems for high-performance superconducting applications.

2 Experimental procedure

In this study, bulk ceramic superconductors with the nominal composition $Bi_2Sr_2Ca_{1-y}Na_yCu_{2-x}Li_xO_8$ (where y = 0.00, 0.05 and x = 0.00, 0.05, 0.10, 0.15, 0.20) were fabricated using the conventional solid-state reaction method. Precisely measured stoichiometric proportions of high-purity raw materials, namely Bi_2O_3, CuO, $SrCO_3$, $CaCO_3$, Na_2CO_3, and Li_2CO_3 were thoroughly ground in an agate mortar to ensure uniform mixing. The resulting powder mixture underwent a two-step

calcination process: first at 750 °C for 12 h, followed by regrinding and a second heating stage at 800 °C for another 12 h. After natural cooling and additional grinding, the powders were compressed into disc-shaped pellets (1.3 cm in diameter, 2 mm thick) using a hydraulic press with an applied pressure of 6 tons/cm^2. The sintering process followed a multi-step thermal profile: an initial heating to 795 °C at 5 °C/min, further increased to 850 °C at 1 °C/min, held at 850 °C for 60 h, then gradually cooled to 795 °C at 1 °C/min, maintained at this temperature for 12 h, and finally quenched to ambient conditions. Post-sintering, the samples were characterized using multiple analytical techniques. Phase composition, crystallinity, and lattice parameters were examined by X-ray diffraction (XRD) on a PANalytical Empyrean system with Cu-Kα radiation ($\lambda = 1.54$ Å), over a 2θ scan range from 5° to 60° at room temperature. Microstructural and surface features were investigated using a FEI-Quanta FEG 650 scanning electron microscope (SEM) coupled with energy dispersive spectroscopy (EDS). Electrical transport properties under magnetic fields up to 5 T were measured using a Physical Property Measurement System (*PPMS*) employing the four-probe method. Furthermore, magnetic hysteresis (*M–H*) loops were recorded with the same system to evaluate flux pinning effects and current transport behavior. The samples with the nominal composition $Bi_2Sr_2Ca_{1-y}Na_yCu_{2-x}Li_xO_8$ (x = 0.00, 0.05; y = 0.00, 0.05, 0.10, 0.15, 0.20) are referred to throughout the text as Na00-Li00 (x = 0.00, y = 0.00), Na05-Li00 (x = 0.05, y = 0.00), Na05-Li05 (x = 0.05, y = 0.05), Na05-Li10 (x = 0.05, y = 0.10), Na05-Li15 (x = 0.05, y = 0.15), and Na05-Li20 (x = 0.05, y = 0.20), respectively.

3 Results and discussion

Figure 1 illustrates the room temperature X-ray diffraction (*XRD*) patterns of undoped and Na-Li co-doped Bi-2212 samples collected in the 2θ range from 5° to 60°. A general examination of the patterns reveals that the all samples exhibit remarkably similar peak profiles, with the Bi-2212 phase (marked as "2") clearly dominating in each case. Minor reflections corresponding to the Bi-2201 (marked as "1") and Bi-2213 (marked as "3") phases are also detected with very low intensity (< 5%).No distinct peaks associated with Na- or Li- containing oxides (such as Na_2O, Li_2O, or $LiCuO_2$) were observed even at high sensitivity scans, confirming that Na^+ and Li^+ are incorporated into the Bi-2212 lattice rather than forming separate impurity phases [45]. The presence of a predominant Bi-2212 phase with trace secondary reflections is typical for polycrystalline Bi-based superconductors and does not significantly influence the superconducting

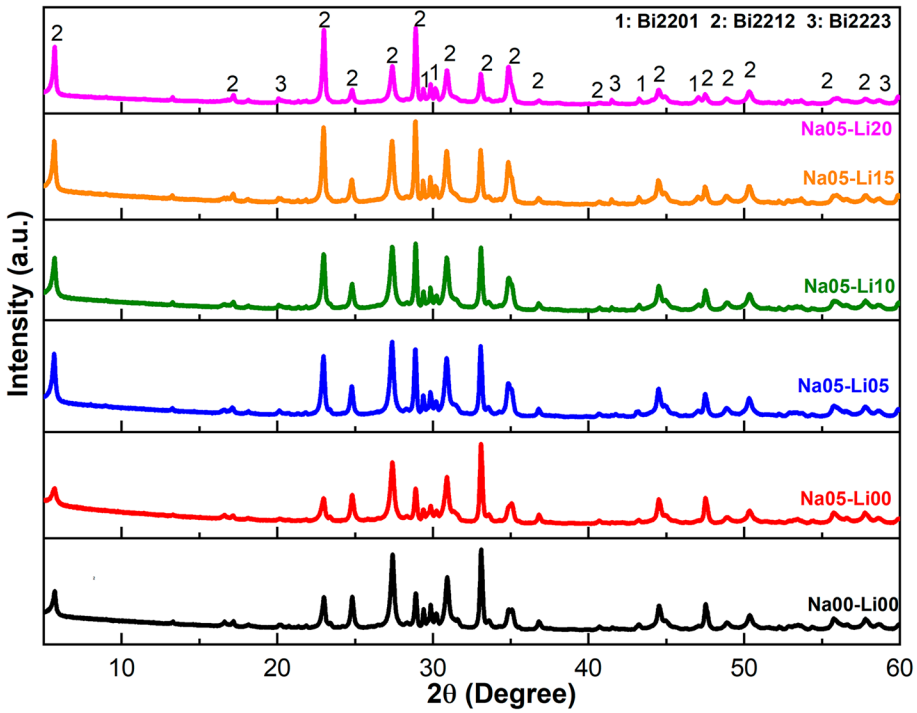


Fig. 1 XRD Patterns of Pure and Na–Li Co-Doped Bi-2212 Samples

characteristics. In particular, the sharpness of the main *(00 l)* reflections and the absence of additional unidentified peaks indicate that phase purity is maintained across the doping series. This suggests that the observed improvements in superconducting properties mainly originate from intrinsic lattice modifications caused by Na and Li co-substitution rather than from secondary phase effects.

When evaluating the differences between the samples, the three most intense peaks for the undoped sample are located at 2θ = 33.09°, 27.42°, and 30.94°, corresponding to the (110), (015), and (017) Miller indices, respectively—all of which correspond to non-(*00 l*) type reflections. Upon the introduction of Na and Li, a clear redistribution of peak intensities is observed, with the intensities of non-(*00 l*) reflections decreasing, while those of (*00 l*)-oriented reflections increase. For instance, in the Na05-Li10 sample, the most intense reflection is indexed to the (00$\underline{1}$0) plane, appearing at 2θ = 28.85°. Similarly, in the Na05-Li15 sample, the three most intense peaks are located at 2θ = 28.85°, 23.01°, and 5.73°, corresponding to the (00$\underline{1}$0), (008), and (002) reflections, respectively. These observations indicate that the incorporation of Na^+ and Li^+ cations enhances the preferential orientation along the *c*-axis, thereby promoting the growth of (*00 l*)-type planes within the Bi-2212 structure, which is commonly associated with improved grain alignment and anisotropic superconducting transport.

The *XRD* peaks corresponding to the Bi-2212 phase were indexed using a tetragonal structure belonging to the *P4/mmm* space group. Lattice parameters were calculated based on the equation:

$$\frac{1}{d^2} = \frac{h^2}{a^2} + \frac{k^2}{b^2} + \frac{l^2}{c^2} \tag{1}$$

In this formula, *d* denotes the spacing between crystal planes, while *h*, *k*, and *l* are the Miller indices, and *a*, *b*, and *c* refer to the unit cell parameters. The lattice parameters of $Bi_2Sr_2Ca_{1-y}Na_yCu_{2-x}Li_xO_8$ show a systematic variation with Li doping, as presented in the Table 1. The in-plane parameter (*a* = *b*) increases gradually from 5.4107 Å for the undoped sample to 5.4193 Å for the highest Li-doped composition (Na05-Li20), while the c-axis parameter shows a slight but consistent elongation from 30.9576 Å to 30.9681 Å. Although the total change in both parameters is relatively small, the monotonic trend confirms that Li is effectively incorporated into the Bi-2212 lattice. Similar linear increases in the *c*-axis with Li concentration have been reported in earlier studies, supporting the conclusion that Li enters the crystal structure successfully [46]. Considering the ionic radii of the constituent cations ($Cu^{2+} < Li^{+1} < Ca^{2+} < Sr^{2+} < Bi^{3+}$), Li is most likely to substitute for Cu sites, leading to a minor lattice expansion [47]. The slight elongation of the *c*-axis can be attributed to a reduction in oxygen content associated with Li incorporation. During synthesis, Li_2O partially replaces CuO, resulting in a small decrease in oxygen stoichiometry and a corresponding increase in the interlayer spacing [46]. Furthermore, it was also indicated that Li addition without Cu removal produces strong CuO impurity peaks, while Li addition accompanied by Cu reduction yields a typical Bi-2212 diffraction pattern with Li retained in the crystal and Cu deficiency observed within the grains, confirming that Li ions occupy the Cu site [38, 46].

Additionally, the average crystallite size (*D*) was estimated using the Debye–Scherrer equation given as [48]:

$$D = \frac{K\lambda}{\beta \cos\theta_\beta} \tag{2}$$

In this equation, λ represents the wavelength of the incident X-ray radiation, β denotes the full width at half maximum (FWHM) of the selected diffraction

Table 1 Key Structural and Electrical Transport Parameters of the Samples

Sample	a ≈ *b*(Å)	c (Å)	*D* (nm)	ρ_0 (mΩ.cm)	ρ_{95K} (mΩ.cm)	T_c^{onset} (K)	T_c^{offset} (K)					ΔT_c (K)
							0 T	0.5 T	1 T	3 T	5 T	
Na00-Li00	5.4107	30.9576	41.33	44.35	53.97	81.6	71.10	60.10	54.30	44.20	38.05	10.5
Na05-Li0	5.4138	30.9558	49.62	36.52	46.10	82.9	74.58	64.52	60.79	52.21	47.50	8.3
Na05-Li05	5.4155	30.9603	55.51	4.41	7.52	83.1	75.15	65.47	62.25	53.65	48.64	7.9
Na05-Li10	5.4163	30.9636	59.90	1.59	3.68	85.4	75.28	63.58	58.98	50.16	45.23	10.1
Na05-Li15	5.4174	30.9652	59.48	2.29	4.35	85.1	75.36	62.80	58.16	48.89	43.84	9.7
Na05-Li20	5.4193	30.9681	49.82	18.51	27.26	81.9	75.52	61.81	56.36	46.47	41.05	6.4

peak, and θ_β corresponds to the Bragg angle. For each specimen, the three most intense diffraction peaks were employed in the calculation, and the final crystallite size (D) was obtained by averaging the individual results. According to the results in Table 1, the crystallite size ranges from 41.33 to 59.90 nm and shows a slight increasing trend with rising Li content up to a 10% substitution level.

To investigate the microstructural characteristics of the samples, scanning electron microscopy (SEM) images were acquired for all specimens using secondary electron (SE) mode at an accelerating voltage of 20 kV and a magnification of 10KX, as presented in Fig. 2. SEM analysis enables the evaluation of various physical features, including grain morphology and alignment, micro-voids, porosity, and the connectivity between grains. From the SEM micrographs, it is evident that all samples are composed of randomly oriented, plate-like grains along with sporadic microstructural voids. This morphology is recognized as a typical feature of Bi-2212 synthesized via the solid-state reaction route [49]. Furthermore, the SEM images reveal that the presence of Na and Li promotes grain growth, as reflected by the increase in grain size.

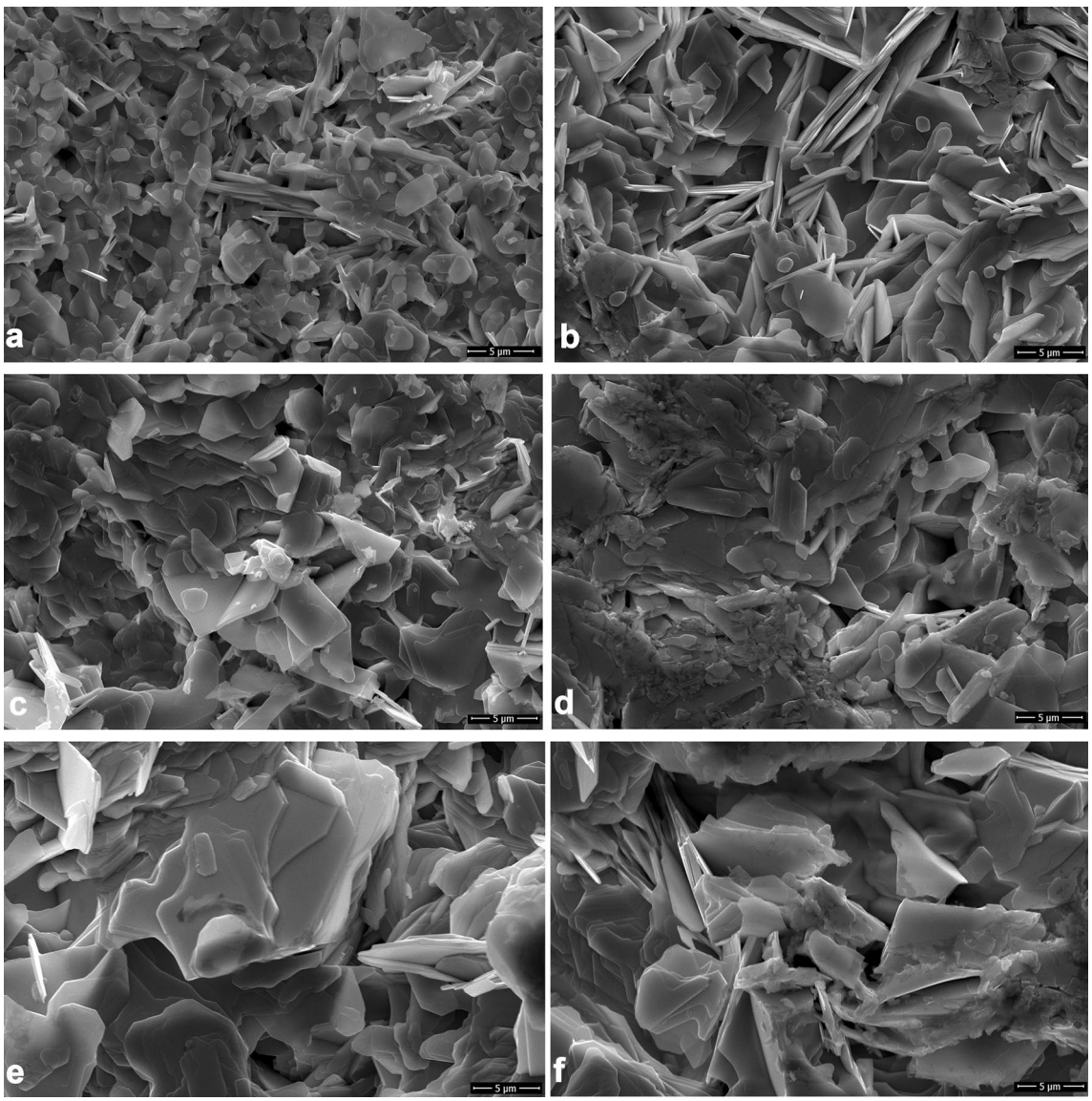


Fig. 2 SEM images of the samples taken at 10KX magnification: **a** Na00-Li00, **b** Na05-Li00, **c** Na05-Li05, **d** Na05-Li10, **e** Na05-Li15, and **f** Na05-Li20

In samples with higher Li content, partially melted regions are also observed, indicating local melting during synthesis. The presence of Li in the Bi-2212 system appears to lower the crystallization temperature, thereby facilitating the formation of larger grains. Literature reports support these findings, noting that the incorporation of alkali metals, particularly lithium, into BSCCO systems can reduce the melting point and the formation temperature of the Bi-2212 phase [35]. This modification improves the intergranular connectivity by reducing voids at grain boundaries and can enhance the superconducting transition temperature (T_c) as well. Additionally, expanded molten regions observed in the micrographs suggest improved grain connectivity, which enhances the coupling between superconducting grains [27]. The local elemental composition of the Bi-2212 samples was examined using energy dispersive spectroscopy (EDS), with results for the Na00-Li00 and Na05-Li20 samples shown in Fig. 3. Since Li is a very light element, it is not detectable by EDS [50]; however, all other expected elements were detected, and no additional elements were observed, indicating the absence of contamination. EDS measurements for Na00-Li00 sample contains Bi 34.73 wt%, Sr 25.55 wt%, Ca 3.93 wt%, Cu 13.17 wt%, and O 22.61 wt%. While the Sr content matches the nominal stoichiometry, Bi, Ca, and Cu are slightly lower than expected. Such deviations are commonly observed in Bi-2212 ceramics and are likely due to local compositional inhomogeneity including regions with lower Bi and Cu content (which are present in all samples) [51], indicated by black areas in the SEM images (arrow #1, Fig. 3e). The relatively high measured oxygen content can be attributed to surface oxidation and the limited quantification accuracy of EDS for light elements. In Li-doped samples, a slight decrease in oxygen concentration is observed (Fig. 3d), suggesting that Li incorporation promotes oxygen deficiency or modifies the oxygen coordination environment, consistent with previous reports and the observed increase in the c-axis parameter from XRD analysis [46]. Overall, the results indicate that the samples preserve the Bi-2212 phase composition, with minor elemental and microstructural variations typical of polycrystalline BSCCO ceramics.

The DC resistivity as a function of temperature, recorded in the range of 15 K to 150 K for all synthesized samples, is depicted in Fig. 4. The figure clearly illustrates that, variations in Na and Li content lead to pronounced modifications in the electrical resistivity behavior, providing strong evidence for the effective incorporation of Na and Li into the Bi-2212 matrix. The resistivity curves reveal three clearly distinct temperature regions. At higher temperatures, a nearly linear increase in resistivity with temperature is observed, representing the normal metallic behavior. As the temperature drops further, a nonlinear deviation appears due to the emergence of superconducting fluctuations associated with the formation of Cooper pairs. At lower temperatures, the resistivity drops sharply toward zero, indicating the development of global phase coherence among the Cooper pairs due to enhanced interlayer coupling. Based on these characteristic regions, several key transport parameters are extracted: residual resistivity (ρ_o), resistivity at 95 K (ρ_{95K}), and the onset (T_c^{onset}) and offset (T_c^{offset}) superconducting transition temperatures. For the higher-temperature metallic region (above (ρ_{95K}), resistivity follows a nearly linear decline with temperature ($d\rho/dT < 0$), which reflects metallic-like behavior. This linear section can be effectively analyzed using Matthiessen's rule:

$$\rho = \rho_0 + \rho_{ep} \tag{3}$$

Here, ρ_o denotes the temperature-independent resistivity component, primarily arising from structural defects, including vacancies, dislocations, grain boundary irregularities, and disoriented CuO_2 planes. Conversely, ρ_{ep} corresponds to the temperature-dependent portion, predominantly associated with electron–phonon scattering mechanisms [52–54]. The values of ρ_o are determined by extrapolating the linear part of the high-temperature region of each curve, as shown in Fig. 4. According to Table 1, the pristine sample (Na00-Li00) exhibits a ρ_o value of 44.35 mΩ·cm. Introducing 0.05Na leads to a noticeable drop in this value, and as Li content increases, ρ_o reaches its minimum (1.59 mΩ·cm) for the Na05-Li10 composition. However, further Li incorporation reverses this trend, increasing ρ_o to 18.51 mΩ·cm in Na05-Li20. The pronounced reduction in ρ_o at optimal doping levels suggests a suppression of lattice disorder and improved structural homogeneity, resulting from the synergistic effect of Na and Li co-doping.

Another crucial parameter is the resistivity measured at 95 K (ρ_{95K}), which reflects the combined impact of impurity scattering and lattice strain fields

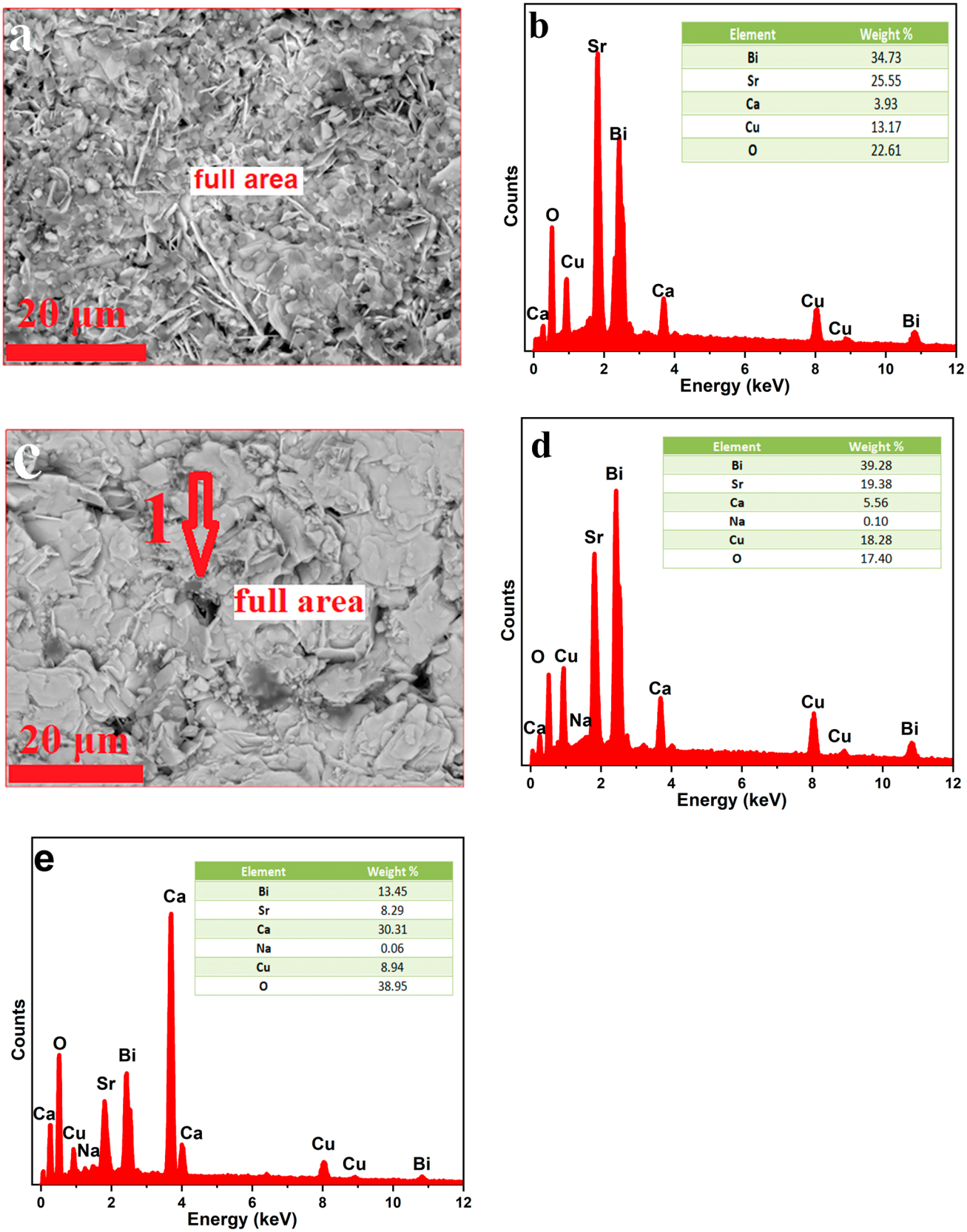


Fig. 3 **a** Selected areas of Na00-Li00 for EDS measurement, **b** EDS results for Na00-Li00, **c** Selected areas of Na05-Li20 for EDS measurement, **d** EDS results for Na05-Li20, and **e** EDS results for black regions (arrow #1)

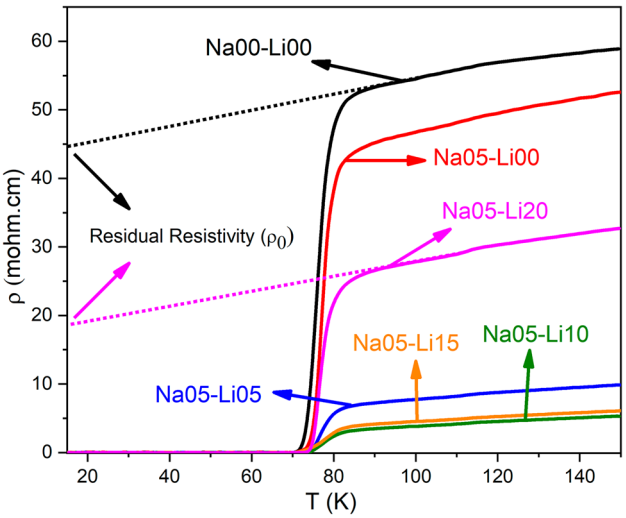


Fig. 4 Temperature dependence of resistivity for all samples

[55]. A trend similar to ρ_o is observed: ρ_{95K} initially decreases from 53.97 mΩ.cm to a low of 3.68 mΩ.cm as Li content increases (up to x = 0.10), followed by a rise to 27.26 mΩ.cm in Na05-Li20. This suggests that co-doping with Na and Li not only improves grain connectivity but also alleviates microstructural irregularities, enhancing metallic intergranular pathways.

The influence of Na-Li co-doping on the onset and offset superconducting transition temperatures, denoted as T_c^{onset} and T_c^{offset}, was evaluated based on the DC resistivity measurements. T_c^{onset} marks the point where superconductivity first emerges within isolated grains (intra-grain regions), typically indicated by the deviation from metallic conductivity and the beginning of a sharp resistivity decline [56]. In contrast, T_c^{offset} is associated with the final stage of the superconducting transition, representing the point where inter-grain coherence is established and the material attains near-zero resistance. This parameter offers insights into the extent of superconducting volume and the connectivity across grain boundaries [57]. T_c^{onset} and T_c^{offset} values for all samples (at 0 T) are tabulated in Table 1. A clear trend is observable: T_c^{onset} increases consistently from 81.6 K for the undoped sample to a peak of 85.4 K in the Na05-Li10 composition, after which it gradually declines, reaching 81.9 K at x = 0.20 (Na05-Li20). A comparable progression is seen in the T_c^{offset} values. The initial improvement in these transition temperatures can be attributed to enhanced carrier concentration within the CuO_2 planes, increased pairing strength (Ψ_o), improved connectivity among superconducting domains, and more uniform oxidation states across the structure [58]. The ΔT_c values were determined from the resistivity measurements (ρ–T curves) and are presented in Table 1. The undoped sample (Na00–Li00) exhibits a relatively broad transition with $\Delta T_c \approx 10.5$ K, whereas the co-doped samples generally show narrower transitions (e.g., Na05–Li05 $\Delta T_c \approx 7.9$ K and Na05–Li20 $\Delta T_c \approx 6.4$ K), indicating improved phase uniformity and better intergranular coupling compared to the undoped material.

In Type II superconductors, magnetic vortex lines penetrate the material when the external magnetic field exceeds the lower critical field (H_{c1}). Under these conditions, applying a current density $\boldsymbol{J}$ generates a Lorentz force $\boldsymbol{F_L} = \boldsymbol{J} \times \boldsymbol{B}$, which acts on the vortices and causes them to move. This vortex motion induces dissipation and leads to a finite resistance. To suppress this motion, pinning centers must be introduced within the material to counterbalance the Lorentz force. These centers are typically associated with structural imperfections such as microstructural inhomogeneities, dislocation networks, and grain boundaries. When effective pinning is achieved, vortex mobility is reduced, thereby minimizing energy losses. However, even under strong pinning conditions, thermally activated flux creep may occur at elevated current densities, causing vortices to hop between pinning sites [59]. Additionally, as the temperature approaches the critical temperature, vortex motion can take place even at very low current densities ($J << J_c$) [60]. Resistivity measurements under varying magnetic fields offer valuable information regarding flux dynamics and pinning efficiency. In this respect, magneto-resistivity measurements were performed between 10 and 150 K in magnetic fields of 0, 0.5, 1, 3, and 5 T, with the resulting resistivity curves shown in Fig. 5. From these curves, the corresponding T_c^{onset} and T_c^{offset} values were extracted and compiled in Table 1.

As the T_c^{onset} temperatures show negligible dependence on the applied magnetic field, only the zero-field results are presented. In contrast, a marked suppression in T_c^{offset} is observed as magnetic field strength increases, which is a well-established characteristic of the Bi-2212 system. This behaviour indicates that the applied magnetic field primarily affects intergranular superconducting pathways, weakening the coherence between grains and thereby limiting long-range superconducting current transport [61].

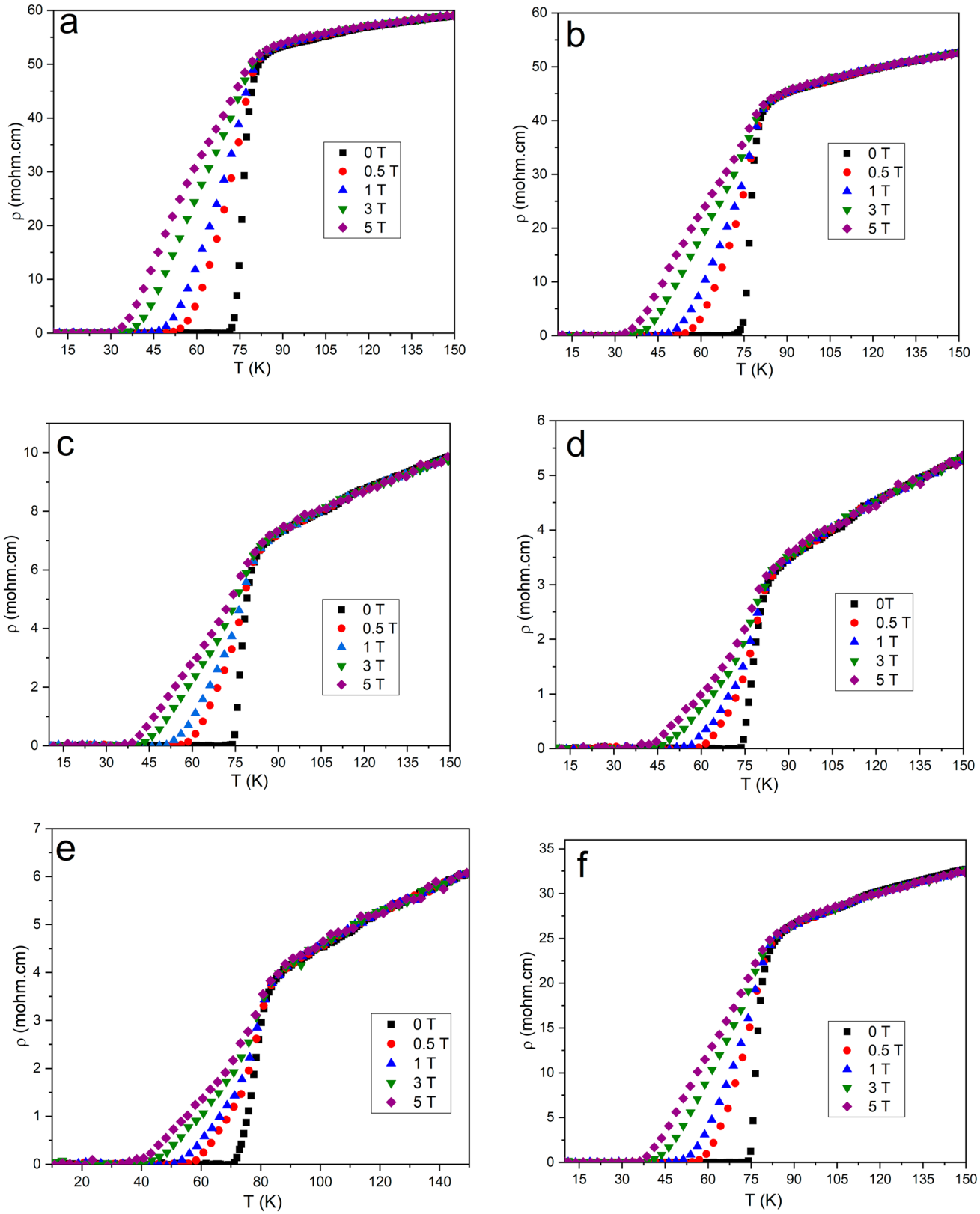


Fig. 5 Magneto-resistivity curves for **a** Na0-Li0, **b** Na05-Li0, **c** Na05-Li05, **d** Na05-Li10, **e** Na05-Li15, **f** Na05-Li20

The low-temperature region of the resistivity data progressively broadens with increasing magnetic field strength, reflecting a weakening of interlayer coupling and a corresponding shift of superconducting transitions to lower temperatures. For instance, T_c^{offset} drops from 71.10 K to 38.05 K in the undoped sample, while in the Na05-Li10 sample it decreases from 75.28 K to 45.23 K. Overall, the Na-Li doped compositions consistently demonstrate higher T_c^{offset} values than the pristine material, indicating enhanced interlayer connectivity and reduced lattice imperfections resulting from alkali doping [62, 63].

This field-induced shift in the resistivity curves is consistent with the thermally activated flux flow (TAFF) mechanism, which is described by the relation:

$$\rho(H,T) = \rho_0 \exp\left(-\frac{U(H)}{k_B T}\right) \quad (4)$$

In this formula, U represents the vortex pinning activation energy, k_B is Boltzmann's constant, and ρ_0 denotes the pre-factor. Since the activation energy vanishes above T_c^{onset}, it is reasonable to approximate ρ_0 using the resistivity at 90 K [60]. The dependence of U on magnetic field is shown in Fig. 6, where U values are obtained from the slope of the linear region in the $ln(\rho/\rho_0)$ versus $1/T$ presented in Fig. 7 (representative curves for the Na00–Li00 and Na05–Li10 samples are included for clarity). With increasing magnetic field strength, the low-temperature region of the resistivity gradually shifts toward lower temperatures and the linear slope becomes shallower, indicating a reduction in U. This decrease is pronounced at low fields (up to 1 T), followed by a more gradual reduction between 1 and 5 T giving rise to a mesa-like behavior. At lower magnetic fields, flux penetration occurs predominantly through weakly coupled grain boundaries, rapidly suppressing superconducting links and reducing the activation energy. At higher fields, flux lines increasingly penetrate the intra-grain regions, where stronger pinning dominates, resulting in a saturation-like response of U [64]. Notably, all Na-Li doped samples exhibit higher U values compared to the undoped specimen, suggesting enhanced vortex pinning due to either stronger pinning potentials or an increased density of effective pinning centers. Moreover, the ability of the magnetic field to permeate the intergranular regions is closely linked to the nature and distribution of weak links between superconducting clusters. The improved connectivity in the doped

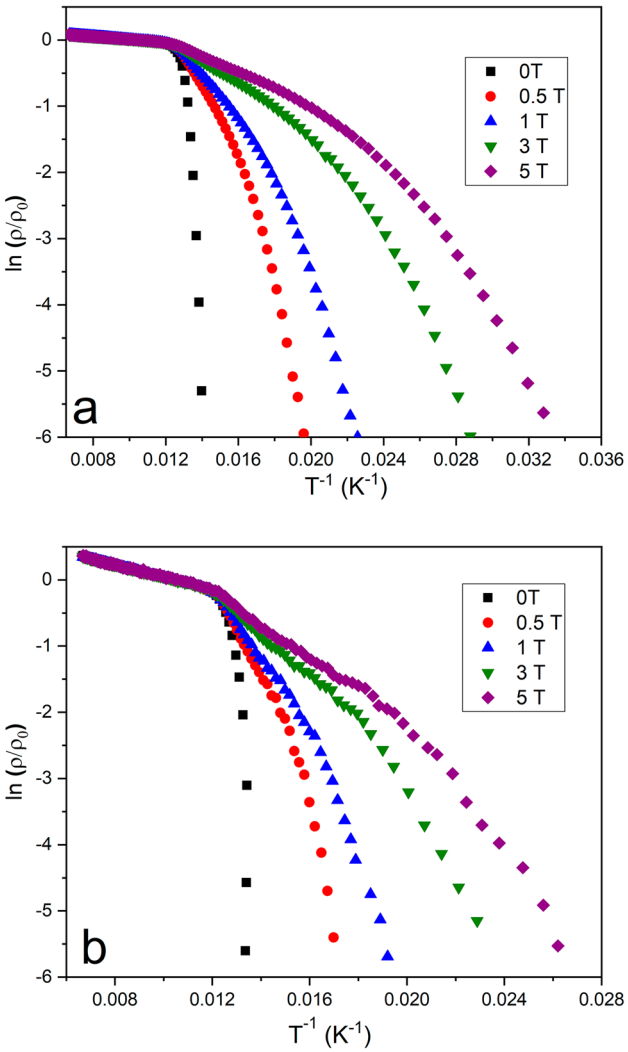


Fig. 6 $ln(\rho/\rho_0)$ versus $1/T$ plots for **a** Na00-Li00 and **b** Na00-Li05

samples, particularly in Na05-Li10 indicates more robust inter-cluster coupling relative to the undoped material [65].

Another important parameter derived from magneto-resistivity measurements is the irreversibility field (H_{irr}). It signifies the magnetic field at which the superconducting phase persists, but the magnetization (M-H) loop becomes reversible due to the onset of vortex motion. In this regime, the vortex pinning weakens, allowing vortices to depin and move freely, thus causing the magnetization hysteresis to vanish. H_{irr} is particularly important for practical applications, as it correlates strongly with the maximum sustainable critical current. In high-Tc superconductors, current-carrying capability diminishes rapidly

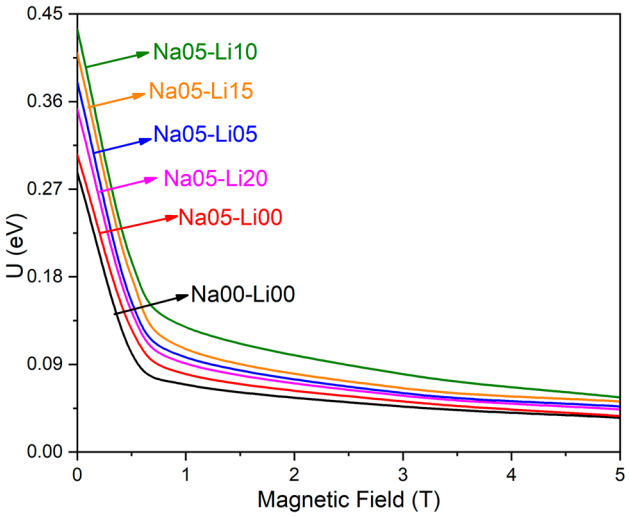


Fig. 7 Activation energies (U) for Na–Li co-doped Bi-2212 sample

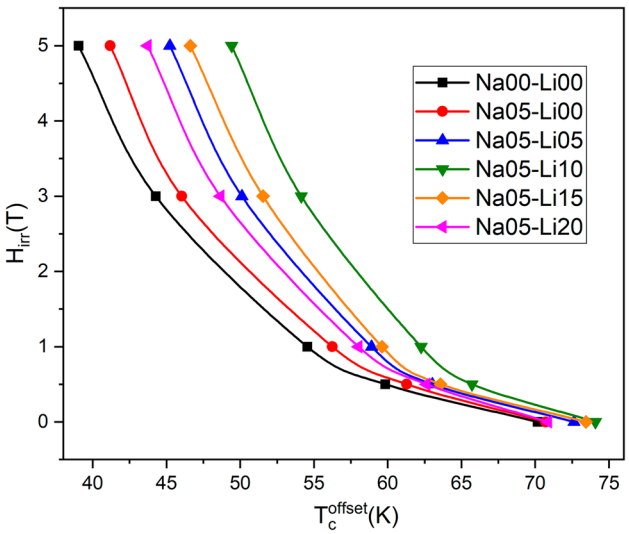


Fig. 8 Irreversibility field (H_{irr}) as a function of T_c^{offset} curves for all samples

as magnetic reversibility emerges. Determining H_{irr} allows for the construction of the irreversibility line (*IL*), which marks the boundary between the vortex glass and vortex liquid phases in the phase diagram. Plotting H_{irr} as a function of the irreversibility temperature T_{irr} establishes the *IL*. At higher temperatures, where $T_{irr} < T < T_c^{onset}$ and $H_{irr} < H < H_{c2}$ thermal fluctuations dominate over pinning, leading to ohmic behavior and reversible magnetism. Below T_{irr}, however, flux pinning becomes effective, and vortex dynamics are frozen, resulting in irreversible magnetic behavior due to flux trapping.

To map the *IL* for the synthesized materials, H_{irr} with respect to T_c^{offset} plots (Fig. 8) were utilized [66]. These curves indicate that samples co-doped with Na and Li display a noticeable upward shift in their *IL* compared to the undoped specimen, suggesting enhanced interlayer connectivity and stronger flux pinning in the doped samples. This improved vortex immobilization points to better superconducting performance in the modified Bi-2212 system.

The extrapolated H_{irr} values at 0 K are summarized in Table 2 and show a clear increase with doping, reaching a maximum of 25.94 T for the Na05-Li10 composition corroborating earlier conclusions regarding enhanced coupling and vortex pinning efficiency.

In addition, upper critical field **(H_{c2})** values were derived from resistivity data using the temperature where the resistivity reached 50% of its normal-state value at 95 K, corresponding to the midpoint transition temperature T_c^{mid} [65]. The H_{c2} vs. T_c^{mid} plots (Fig. 9) clearly show that the curves shift toward higher temperatures with increasing dopant levels, in agreement with the H_{irr} vs. T_c^{offset} trends.

The upper critical field at absolute zero, $H_{c2}(0)$, was determined by the Werthamer–Helfand–Hohenberg (WHH**)** relation [67]:

Table 2 Summary of critical fields, coherence length, penetration depth, and remanent magnetization

Sample	H_{irr} (0) (T)	H_{c2} (0) (T)	$\xi(0)$ (Å)	λ (0) (Å)	M_R (emu/cm^3)		
					10 K	**20 K**	**30 K**
Na00-Li00	17.32	19.41	41.23	43.63	9.88	4.56	2.91
Na05-Li0	22.02	24.08	36.98	38.68	11.46	5.17	3.35
Na05-Li05	23.53	29.89	33.19	37.41	17.06	8.95	5.68
Na05-Li10	25.94	48.55	26.04	35.63	22.14	10.19	6.37
Na05-Li15	23.91	42.25	27.92	37.12	19.15	9.25	5.86
Na05-Li20	22.71	24.85	36.41	38.08	16.35	8.23	5.22

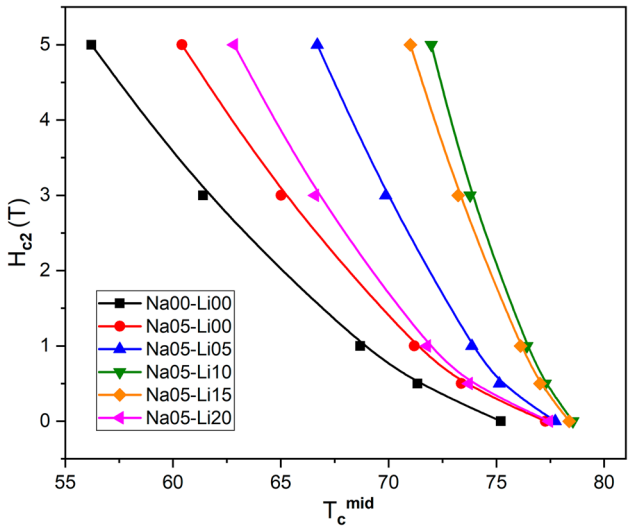


Fig. 9 Upper critical field (H_{c2}) as a function of T^{mid} curves for all samples

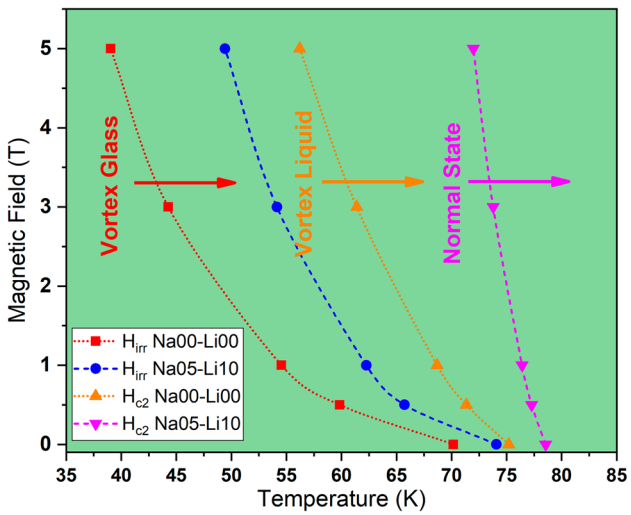


Fig. 10 Vortex Glass, Vortex Liquid and Normal State region for Na00-Li00 and Na05-Li10 samples

$$H_{c2} = -0.693 T_c \left(\frac{dH_{c2}}{dT} \right) \tag{5}$$

The computed $H_{c2}(0)$ parameters are listed in Table 2, showing a progressive enhancement with doping, peaking at 48.55 T for the Na05-Li10 sample. This further demonstrates that another key superconducting property of Bi-2212 has been positively influenced through Na-Li incorporation.

Using the H_{irr} and H_{c2} curves, the regions corresponding to the vortex glass, vortex liquid, and normal states are sketched in Fig. 10 for both the undoped (Na00–Li00) and Na05–Li10 samples [66]. The Na–Li co-doped sample displays a clear enhancement in both the irreversibility field and the upper critical field, shifting the H_{irr} and H_{c2} lines toward higher temperatures and magnetic fields. This indicates an expansion of the vortex glass and vortex liquid regions, effectively suppressing the transition to the normal state. The enlarged vortex glass region reflects stronger vortex pinning and improved thermal stability, while the increase in H_{c2} suggests a higher intrinsic superconducting performance. These results confirm that co-doping with Na and Li significantly improves the flux pinning capability and broadens the operable superconducting regime, making the material more suitable for high-field applications.

From the zero-temperature values of $H_{irr}(0)$ and $H_{c2}(0)$, two fundamental superconducting parameters, the coherence length (ξ) and the magnetic penetration depth (λ), can be estimated using the following theoretical expressions [68]:

$$\xi(0) = \left[\frac{\phi_0}{2\pi\mu_0 H_{c2}(0)} \right]^{1/2} \text{and } \lambda(0) = \left[\frac{\phi_0}{2\pi\mu_0 H_{irr}(0)} \right]^{1/2} \tag{6}$$

In these equations, Φ_0 denotes the magnetic flux quantum, valued at 2.07×10^{-15} T·m^2. Using these relations, the corresponding ξ and λ values for all compositions were calculated and are reported in Table 2 The results reveal a decreasing trend in both parameters with increasing Na-Li content. Specifically, the Na05-Li10 sample exhibits the most compressed superconducting state, with a minimum coherence length of 26.04 Å and a penetration depth of 35.63 Å. This reduction indicates stronger flux pinning and improved superconducting coupling in the doped material.

Figure 11 displays the magnetic hysteresis (M–H) curves of pure and Na05-Li10 samples were recorded at magnetic field sweeps between –2 and + 2 T, at temperatures of 10, 20, and 30 K. The M–H curves clearly demonstrate sensitivity to both the level of Na–Li doping and the measurement temperature. A key observation is that all curves exhibit symmetry and reversibility, implying that flux line dynamics are governed predominantly by bulk pinning mechanisms rather than surface barriers.

With increasing temperature, the area enclosed by the M–H loops reduces for all samples, indicating weaker superconducting interconnectivity and diminished grain coupling. Nevertheless, upon Na–Li co-doping,

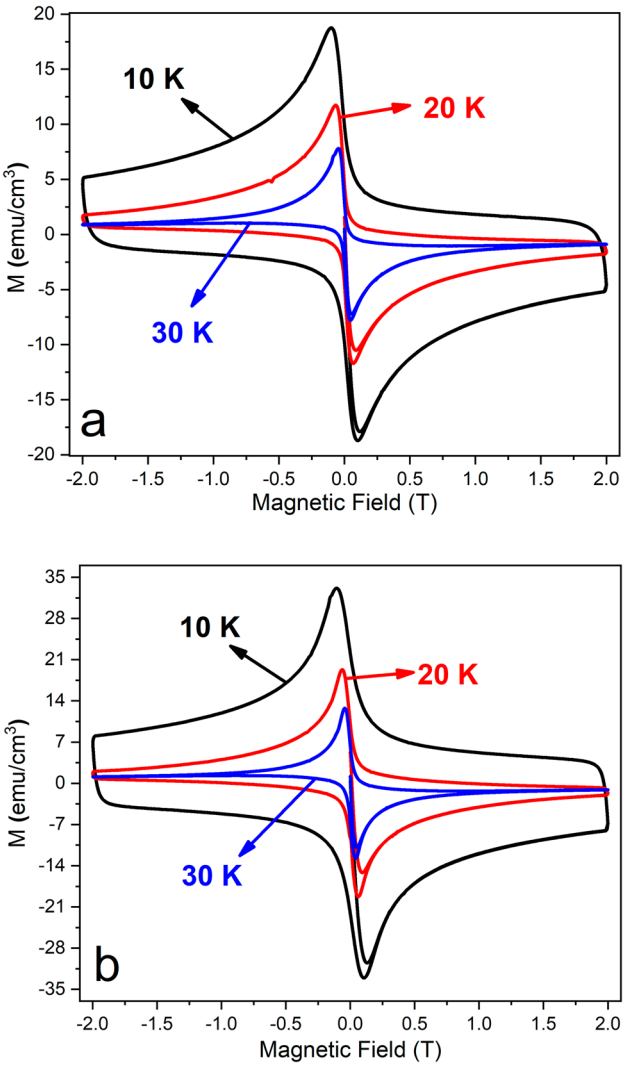


Fig. 11 M-H Loops of **a** Na00-Li00 and **b** Na05-Li10

the *M–H* loops become noticeably broader at all temperatures, suggesting enhanced flux pinning and increased magnetic irreversibility. Additionally, the remanent magnetization (M_R), an indicator of trapped magnetic flux, was extracted from the zero-field intercepts of the *M–H* loops and summarized in Table 2. These values show a consistent decline with rising temperature, reflecting a decrease in the overall pinning efficiency [69]. Despite this, all doped samples show noticeably higher M_R values compared to the undoped counterpart. It can be said that the introduction of Na^+ and Li^+ ions likely introduces additional point defects and local lattice distortions within the Bi-2212 matrix, which act as effective pinning centers. These defects hinder vortex motion more efficiently, thereby enhancing the material's ability to carry supercurrents under applied

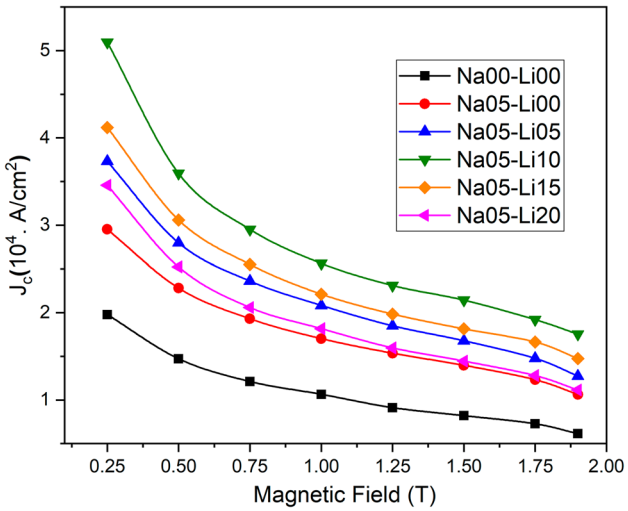


Fig. 12 Critical Current Density (J_c) of All Samples at 10 K

magnetic fields. This enhancement in vortex pinning highlights alkali-metal co-doping as an effective and viable strategy for optimizing the superconducting performance of Bi-based cuprates.

The intra-grain critical current densities (J_c) for all specimens at 10 K were estimated from the magnetization (M) versus magnetic field (H) curves using Bean's critical state model [70], expressed as:

$$J_c = \frac{20\Delta M}{\left[a\left(1-\frac{a}{3b}\right)\right]} \tag{7}$$

In this equation, ΔM represents the difference in magnetization (in emu/cm^3) between the ascending (M^{up}) and descending (M^{down}) branches of the hysteresis loop at a specific applied field, while a and b correspond to the sample dimensions perpendicular to the field direction. Figure 12 shows how J_c varies between 0.25 T and 2 T. The plot clearly shows that co-doped samples demonstrate higher J_c values compared to the undoped sample. This suggests that the incorporation of Na and Li into the Bi-2212 matrix leads to improved grain connectivity and refined microstructural features supported by SEM and reduced residual resistivity, thereby facilitating better current transport across grain boundaries.

The flux pinning force (F_p) of the samples was calculated using the relation:

$$F_p = J_c \times \mu_0 H \tag{8}$$

where J_c is the critical current density and H is the applied magnetic field [71]. Figure 13 compares the

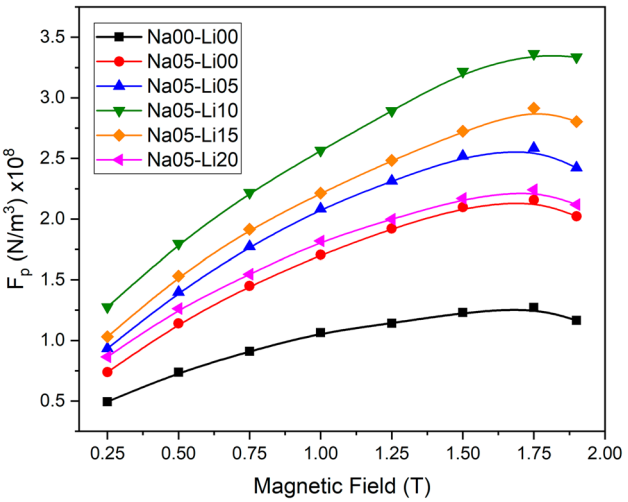


Fig. 13 Variation of pinning force (F_p) with magnetic field for all samples at 10 K

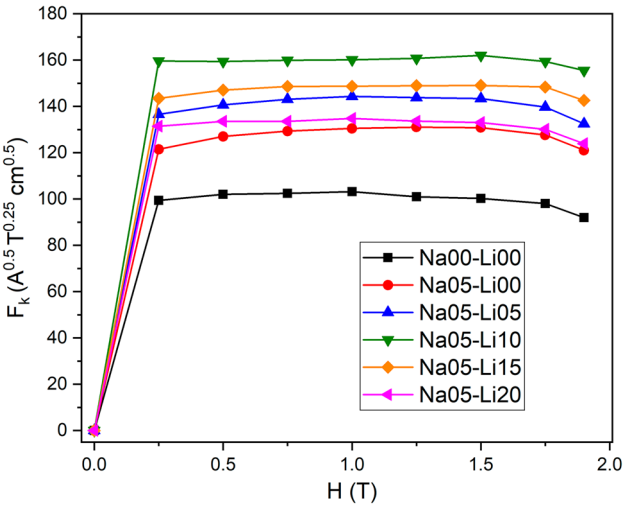


Fig. 14 Kramer plots $F_K = J_c^{0.5} H^{0.25}$ for all samples obtained at 10 K

field dependence of F_p for the pure and Na–Li co-doped Bi-2212 samples. The obtained curves clearly demonstrate that Na–Li co-doping in Bi-2212 significantly enhances the flux pinning capability of the material compared to the undoped sample. This enhancement is attributed to the introduction of additional effective pinning centers created by the Na and Li dopants within the crystal lattice or at grain boundaries. The increased F_p indicates stronger vortex immobilization under applied magnetic fields, which correlates with improved critical current density (J_c) performance. The co-doping likely modifies the microstructure, promoting defects that act as efficient vortex pinning sites. Consequently, the Na–Li doped Bi-2212 can sustain higher supercurrents in magnetic fields, making it more suitable for practical superconducting applications where magnetic flux stability is crucial.

Figure 14 shows the Kramer plots, $F_K = J_c^{0.5} H^{0.25}$, as a function of magnetic field for all samples at 10 K. Kramer analysis is a useful tool to determine the irreversibility field H_{irr} and to gain insight into the flux pinning behavior in type-II superconductors [72, 73]. As seen in the figure, F_K rapidly increases at low fields and then reaches a nearly constant region before gradually decreasing at higher fields, indicating strong flux pinning over a wide field range. The extrapolated H_{irr} values from the Kramer plots are 4.15, 4.62, 4.70, 7.83, 5.56, and 4.88 T for the Na00–Li00, Na05–Li00, Na05–Li05, Na05–Li10, Na05–Li15, and Na05–Li20 samples, respectively. The H_{irr} value reaches its maximum at 7.83 T for Na05–Li10, indicating the strongest flux pinning and highest critical current density in this composition. The enhancement in H_{irr} up to x = 0.10 suggests that moderate Li substitution in the Na-doped Bi-2212 matrix creates effective pinning centers, likely due to improved grain connectivity and an optimal level of lattice distortion that favors vortex pinning. However, at higher Li contents (x ≥ 0.15), a slight reduction in H_{irr} is observed which may be attributed to reduced intergranular coupling or excessive lattice strain that weakens the pinning efficiency. Overall, the Kramer analysis confirms that Na–Li co-doping effectively enhances the flux pinning capability of Bi-2212 ceramics, with Na05–Li10 exhibiting the most promising superconducting performance for high-field applications.

To determine the dominant flux pinning mechanism, the variation of the normalized flux pinning force density (F_p/F_{pmax}) was plotted as a function of the reduced field (H/H_{max}) for the Na05-Li10 sample, as shown in Fig. 15. This sample exhibited the highest pinning force among all investigated samples. The experimental data (black squares) are compared with theoretical predictions for three classical flux pinning models: normal surface pinning (magenta dashed line), normal point pinning (red dashed line), and δk pinning (blue dashed line). The corresponding equations are given as [74, 75]:

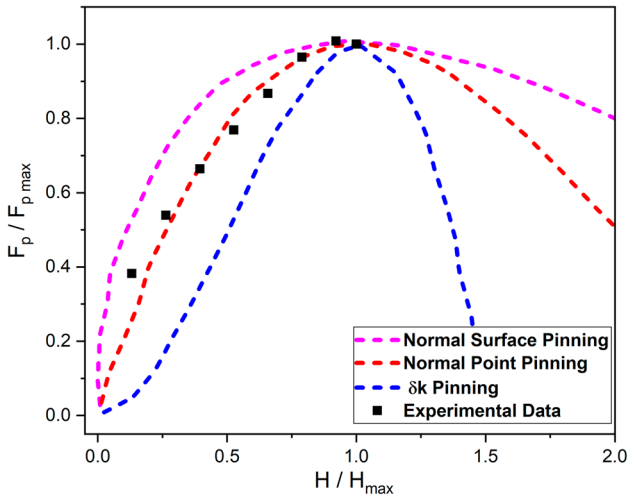


Fig. 15 The variation of the normalized flux pinning density (F_p/F_{pmax}) was plotted as a function of reduced field (H/H_{max}) for Na05-Li10 sample at 10 K

$$f(h) = \frac{25}{16}h^{1/2}\left(1 - \frac{h}{5}\right)^2 \ (normal\ surface\ pinning) \tag{9}$$

$$f(h) = \frac{9}{4}h\left(1 - \frac{h}{3}\right)^2 \ (normal\ point\ pinning) \tag{10}$$

$$f(h) = 3h^2\left(1 - \frac{2h}{3}\right)\ \delta k\ pinning \tag{11}$$

Analysis of the F_p/F_{pmax} scaling indicates that the Na05-Li10 sample exhibits a peak position and curve profile most consistent with the normal point pinning model, suggesting that vortex immobilization is primarily governed by localized nanoscale defects. Quantitatively, the best fit to the Dew-Hughes model $F_p/F_{pmax} = A\ h^p\ (1\text{-}h)^q$ yields parameters $p \approx 1.2$ and $q \approx 2.0$, corresponding to a peak position $h_{peak} = p/(p+q) \approx 0.4$ [73, 76]. This is close to the theoretical value for point pinning ($h_{peak} \approx 0.33$), confirming the predominance of this mechanism. At lower magnetic fields, the experimental curve follows the normal point pinning behaviour, while at higher fields, a slight deviation toward the normal surface pinning trend is observed, indicating a mixed pinning contribution. The presence of both point-like and surface pinning centers suggests that alkali co-doping alters the microstructural defect landscape, increasing the density and distribution of effective pinning centers. This enhanced defect structure improves vortex trapping and consequently increases the critical current density of the Na-Li doped samples compared to the undoped Bi-2212.

4 Conclusion

This study demonstrates that Na–Li co-doping in Bi-2212 superconductors leads to significant enhancement of superconducting performance by improving grain connectivity and introducing effective flux pinning centers. Samples synthesized via the conventional solid-state reaction method showed predominantly the Bi-2212 phase with minor Bi-2201 and Bi-2223 impurities, as confirmed by XRD analysis. SEM images revealed a random grain distribution with increasing grain size correlated to higher Li content. Electrical transport measurements under various magnetic fields indicated that all Na–Li co-doped samples exhibit elevated superconducting transition temperatures (T_c^{onset} and T_c^{offset}) alongside a notable reduction in resistivity. These improvements are attributed to enhanced charge carrier concentration within the CuO_2 planes and strengthened interlayer coupling. Magneto-resistance and magnetic hysteresis analyses further revealed increased activation energies for vortex motion and enhanced vortex pinning, reflected in higher irreversibility fields (H_{irr}), upper critical fields (H_{c2}), critical current densities (J_c), and pinning forces. The combined effects of Na substitution at the Ca site and Li substitution at the Cu site produce a robust superconducting state capable of maintaining structural integrity while overcoming intrinsic limitations of Bi-2212, especially under applied magnetic fields. Among the samples studied, the Li substitution level of x = 0.10 exhibited the most pronounced enhancement in superconducting and magnetic properties. Overall, these findings highlight Na–Li co-doping as a promising and effective strategy for optimizing Bi-2212 superconductors for high-field applications. Future work should focus on fine-tuning the dopant concentrations and further elucidating the underlying flux pinning mechanisms to maximize performance.

Acknowledgements

The authors acknowledge the financial support from the Research Fund of Çukurova University, Adana,

Turkey, through grant contracts No: FDK-2021-13417 and FBA-2023-16367.

Author contributions

F. Karaçora: Software, Data Curation, Material Preparation, Writing—Original Draft. **İ. Ergin:** Software, Data Curation. **M. Gürsul:** Conceptualization, Software, Data Curation, Writing—Review & Editing. **B. Özçelik:** Supervision, Project Administration, Writing—Review & Editing.

Funding

Open access funding provided by the Scientific and Technological Research Council of Türkiye (TÜBİTAK). Çukurova Üniversitesi,FDK-2021-13417,BEKIR OZCELIK,FBA-2023-16367,Mehmet Gürsul

Data availability

Data will be made available on reasonable request.

Declarations

Conflict of interest The author declares no competing interests.

Ethical approval Approval not applicable.

Consent for publication Not applicable.

Open Access This article is licensed under a Creative Commons Attribution 4.0 International License, which permits use, sharing, adaptation, distribution and reproduction in any medium or format, as long as you give appropriate credit to the original author(s) and the source, provide a link to the Creative Commons licence, and indicate if changes were made. The images or other third party material in this article are included in the article's Creative Commons licence, unless indicated otherwise in a credit line to the material. If material is not included in the article's Creative Commons licence and your intended use is not permitted by statutory regulation or exceeds the permitted use, you will need to obtain permission directly from the copyright holder. To view a copy of this licence, visit http://creativecommons.org/licenses/by/4.0/.

References

1. J.G. Bednorz, K.A. Müller, Possible high T_c superconductivity in the Ba–La–Cu–O system. Z. Physik B – Condens. Matter. **64**, 189–193 (1986)
2. M.K. Wu, J.R. Ashburn, C.J. Torng, P.H. Hor, R.L. Meng, L. Gao, Z.J. Huang, Y.Q. Wang, C.W. Chu, Superconductivity at 93 K in a new mixed-phase Y-Ba-Cu-O compound system at ambient pressure. Phys. Rev. Lett. **58**, 908 (1987)
3. H. Maeda, Y. Tanaka, M. Fukutomi, T. Asano, K. Togano, H. Kumakura, M. Uehara, S. Ikeda, K. Ogawa, S. Horiuchi, Y. Matsui, New high-Tc superconductors without rare earth element. Physica C **153**, 602–607 (1988)
4. M. Noe, K.P. Juengst, F.N. Werfel, S. Elschner, J. Bock, F. Breuer, R. Kreutz, Testing bulk HTS modules for resistive superconducting fault current limiters. IEEE Trans. Appl. Supercond. **13**, 1976–1979 (2003)
5. H. Miao, K.R. Marken, M. Meinesz, B. Czabaj, S. Hong, Development of round multifilament Bi-2212/Ag wires for high field magnet applications. IEEE Trans. Appl. Supercond. **15**, 2554–2557 (2005)
6. X.Y. Lu, D. Yi, H. Chen, A. Nagata, Effect of SnO, MgO and Ag_2O mix-doping on the formation and superconducting properties of Bi-2223 Ag/tapes. Phys. Procedia **81**, 129–132 (2016)
7. C. Michel, M. Hervieu, M.M. Borel, A. Grandin, F. Deslandes, J. Provost, B. Raveau, Superconductivity in the Bi-Sr-Cu-O system. Zeitschrift für Physik B Condens. Matter. **68**, 421–423 (1987)
8. J.M. Tarascon, W.R. McKinnon, P. Barboux, D.M. Hwang, B.G. Bagley, L.H. Greene, G. Hull, Y. LePage, N. Stoffel, M. Giroud, Preparation, structure and properties of the superconducting compound series $Bi_2Sr_2Ca_{n-1}Cu_nO_y$ with n = 1, 2, and 3. Phys. Rev. B **38**, 8885 (1988)
9. J. Kumar, D. Sharma, P.K. Ahluwalia, V.P.S. Awana, Enhanced superconducting performance of melt quenched Bi2Sr2CaCu2O8 (Bi-2212) superconductor. Mater. Chem. Phys. **139**, 681–688 (2013)
10. S. Abdelhaleem, M.O. Alziyadi, A. Alruwaili, M.J. Alawi, A. Alkabsh, M.S. Shalaby, BSCCO high Tc -superconductor materials: strategies toward critical current density enhancement and future opportunities. App. Phy. A **13**, 151 (2025)

11. A. Polasek, P. Majewski, E.T. Serra, F. Rizzo, F. Aldinger, Phase relations study on the melting and crystallization regions of the Bi-2223 high temperature superconductor. Mater. Res. **7**, 393 (2004)
12. R.L.C. Manahan, R.V. Sarmago, Growth of superconducting Bi2Sr2CaCu2O8+δ films by sedimentation deposition and liquid phase sintering and annealing technique. Physica C: Supercond. Appl. **445**, 733–736 (2006)
13. S. Zhang, C. Li, Q. Hao et al., Optimized intergrain connection and transport properties of Bi-2212 high-temperature superconductors by Ag nanoparticles inclusions. J. Supercond. Nov. Magn. **28**, 1729–1736 (2015)
14. K.S. Ramesh, M.S.R. Rao, Effect of grain network modifications due to additives on critical current (Ic) in Bi-2212 superconductor. Physica C **316**(1–2), 119–128 (1999)
15. S. Zhang, C. Li, Q. Hao, T. Lu, P. Zhang, Influences of Yb substitution on the intergrain connections and flux pinning properties of Bi-2212 superconductors. Phys. C Supercond. **511**, 26–32 (2015)
16. A. Amira, M.F. Mosbah, P. Molinié, A. Leblanc, Improvement of magnetic properties in Bi-2212 ceramics by fluorine doping. Solid State Sci. **7**(1), 53–57 (2005)
17. A. Sotelo, H. Szillat, P. Majevski, F. Aldinger, Rapid synthesis of the Bi-2212 phase by a polymer matrix method. Supercond. Sci. Technol. **10**, 717 (1997)
18. L. Ben-Dor, M.Y. Szerer, G. Blumberg, A. Givan, L. Börjesson, L.V. Hong, Physical characterization and vibrational spectroscopy of Bi(Pb) cuprate 2212 ceramics prepared by sol-gel. Physica C (1992). https://doi.org/10.1016/0921-4534(92)90396-t
19. A. Bhargava, T. Yamashita, I.D.R. Mackinnon, Manufacture of specific BSCCO powder compositions by co-precipitation. Physica C **247**(3–4), 385–392 (1995)
20. M. Gürsul, C. Özçelik, I. Ergin, M.A. Madre, A. Sotelo, B. Özçelik, Role of Y substitution for Ca-site on magnetoresistivity properties of Bi-2212 superconductor rods prepared by LFZ. Mater. Chem. Phys. **282**, 125995 (2022)
21. M.F. Carrasco, V.S. Amaral, R.F. Silva, F.M. Costa, Electrical assisted laser floating Zone (EALFZ) growth of 2212-BSCCO superconducting fibres. Appl. Surf. Sci. **257**, 5283 (2011)
22. P.M. Sarun, R. Shabna, S. Vinu, A. Biju, U. Syamaprasad, Highly enhanced superconducting properties of Bi-2212 by Y and Pb co-doping. Phys. B Condens. Matter **404**(8–11), 1602–1606 (2009)
23. B. Özçelik, M. Gürsul, A. Sotelo, M.A. Madre, Improvement of superconducting properties in Na-doped BSCCO superconductor. J Mater Sci: Mater. Elec. **26**, 441–447 (2015)
24. W. Labban, W. Malaeb, K. Habanjar, M.S. Hassan, R. Sakagami, Y. Kamihara, R. Awad, Investigations of arsenic substitution on the physical, electrical and magnetic properties of Bi-2212 superconductors. Phase Transit. **93**(10–11), 1055–1066 (2020)
25. S. Zhang, M. Liang, C. Li, Q. Hao, J. Feng, P. Zhang, Enhanced flux pinning properties in Bi-2212 high temperature superconductors with nano-sized precipitates. Mater. Lett. **157**, 197–200 (2015)
26. B. Zhao, W.H. Song, X.C. Wu, J.J. Du, Y.P. Sun, H.H. Wen, Z.X. Zhao, Influence of MgO particle doping on flux pinning in $Bi_2Sr_2CaCu_2O_y$ crystals. Physica C **361**(4), 283–291 (2001)
27. T. Kawai, T. Horiuchi, K. Mitsui, K. Ogura, S. Takagi, S. Kawai, Effect of alkaline metal substitutions to Bi-Sr-Ca-Cu-O superconductor. Phys. C Supercond. **161**(5–6), 561–566 (1989)
28. B. Gopalakrishna, M. Chandra Sekhar, S.V. Suryanarayana, Effect of lithium doping in the Bi-2212 superconducting system. Cryst. Res. Technol. **30**(3), 411–417 (1995)
29. M. Gürsul, Vital variation in superconducting performances of Bi-2212 through lithium substitution. J. Mater. Sci. Mater. Electron. **34**(5), 451 (2023)
30. S. Zhang, C. Li, Q. Hao, X. Ma, T. Lu, P. Zhang, Optimization of Bi-2212 high temperature superconductors by potassium substitution. Supercond. Sci. Technol. **28**(4), 045014 (2015)
31. B. Özçelik, M. Gürsul, A. Sotelo, M.A. Madre, Improvement of the intergranular pinning energy in the Na-doped Bi-2212 superconductors. J. Mater. Sci. Mater. Electron. **26**(5), 2830–2837 (2015)
32. B. Özçelik, M. Gürsul, A. Sotelo, M.A. Madre, Effect of K substitution on structural, electrical and magnetic properties of Bi-2212 system. J. Mater. Sci. Mater. Electron. **25**(10), 4476–4482 (2014)
33. S.-X. Dou, W. Wei-Min, H.-K. Liu, C.C. Sorrell, Mechanism of the Tc enhancement in $Bi_2Sr_2CaCu_2O_{8+y}$ by sodium doping. Physica C: Supercond. **185**, 811–812 (1991)
34. S. Rahier, S. Stassen, R. Cloots, M. Ausloos, Influence of Na doping and sintering temperature on increasing $Bi_2Sr_2CaCu_2O_8$ superconducting phase content in powder-form materials. Mater. Lett. **60**(3), 298–300 (2006)
35. M.P. Volkov, B.T. Melekh, V.I. Bakharev et al., Effect of Li doping on the critical temperature and glass formation in the Bi-Sr-Ca-Cu-O system. Phys. Solid State **41**, 15–17 (1999)
36. I. Matsubara, T. Ogura, H. Yamashita, M. Kinoshita, Y. Hashimoto, T. Kawai, Effects of Li doping on the superconducting properties of Bi-based superconducting whiskers. Phys. C Supercond. **201**(1–2), 83–94 (1992)

37. S. Wu, J. Schwartz, J.C. Rynes, C.A. Gianino, Optimization of processing conditions for bulk ceramic Li doped BSCCO. Appl. Supercond. **1**(1–2), 93–99 (1993)
38. S. Moehlecke, C.H. Westphal, M.S. Torikachvili, J.A. Davis, I.C.L. Torriani, Enhancement of the intergranular superconducting properties in $Bi_2Sr_2CaCu_2O_8$ with Li additions. Physica C **211**(1–2), 113–120 (1993)
39. Y. Yang, J. Xin, X. Xiaonong, S. Jiancang, Y. Xixian, Mechanism of Tc increase in Na-doped $Bi_2Sr_2CaCu_2O_{8+y}$. Chin. Phys. Lett. **11**(1), 46 (1994)
40. A.M. Suvarna, C.S. Sunandana, Magnetic penetration depth in polycrystalline Bi-2212 $Bi_2Sr_2Ca_{1-x}Na_xCu_2O_{8+\delta}$ (x=0–0.3). Physica C **254**(3–4), 355–358 (1995)
41. J.Y. Oh, D.S. Yang, D.H. Tran, B. Kang, Influences of Na-doping on valence states and interatomic potential in $Bi_{1.6}Pb_{0.4}Sr_2Ca_2Cu_3O_{10+\delta}$ superconductor. Ceram. Int. **46**(6), 8259–8263 (2020)
42. R. Wesche, Processing of superconducting powders, in *High-Temperature Superconductors: Materials, Properties, and Applications*, vol. 6, (Springer, Boston, 1998)
43. D.M. Gokhfeld, M.I. Petrov, S.V. Semenov, A.D. Balaev, I.V. Nemtsev, A.D. Vasiliev, M.S. Molokeev, Larger grains in high-Tc superconductors synthesized by the solid-state reaction route. Ceram. Internat. **50**(24), 52213–52217 (2024)
44. D. Dew-Hughes, Model for flux creep in high T_c superconductors. Cryogenics **28**, 674 (1988)
45. D.H. Tran, T.M. Le, T.H. Do, Q.T. Dinh, N.T.T. Duong, D.T.K. Anh, N.K. Man, D. Pham, W. Kang, Enhancements of critical current density in the Bi–Pb–Sr–Ca–Cu–O superconductor by Na substitution. Mater. Trans. **59**(7), 1071 (2018)
46. T. Horiuchi, T. Kawai, K. Mitsui, K. Ogura, S. Kawai, Li substitution in the $Bi_2Sr_2Ca_1Cu_2O_8$ superconductor. Physica C **168**, 309–314 (1990). https://doi.org/10.1016/0921-4534(90)90523-H
47. Y. Fujiwara, S. Hirata, M. Nishikubo, T. Kobayashi, Improved superconductivity in BiSrCaCuO single crystals by lithium doping. IEEE Trans. Magn. **27**(2), 1150–1153 (1991)
48. B.D. Cullity, *Element of X-ray Differaction* (Addison-Wesley Publishing Company Inc., USA, 1956)
49. R. Cabassi, D. Delmonte, M.M. Abbas et al., The role of chemical substitutions on Bi- 2212. Supercond. Crys. **10**, 462 (2020). https://doi.org/10.3390/cryst10060462
50. S.X. Dou, H.K. Liu, W.M. Wu, W.X. Wang, C.C. Sorrell, R. Winn, N. Savvides, Melt processing of alkali element doped $Bi_2Sr_2CaCu_2O_8$. Phys. C **172**, 295–303 (1990)
51. S. Wu, J. Schwartz, G.W. Raban, Superconducting properties and microstructural evolution of Li doped $Bi_2Sr_2CaCu_2O_x$. Physica C **246**, 297–308 (1995)
52. B. Pignon, C. Autret-Lambert, A. Ruyter, R. Decourt, J.M. Bassat, I. Monot-Laffez, L. Ammor, Study of the yttrium and zinc substitutions effects in Bi2Sr2CaCu2O8+δ compounds by transport measurements. Physica C **468**(11–12), 865–871 (2008)
53. P.B. Allen, W. Pickett, H. Krakauer, Anisotropic normal-state transport properties predicted and analyzed for high-Tc oxide superconductors. Phys. Rev. B **37**, 7482 (1988). https://doi.org/10.1103/PhysRevB.37.7482
54. A. Amira, F. Bouaïcha, N. Boussouf, M.F. Mosbah, Substitution of Sr2+ by Eu3+ in Bi-2201 ceramics, effects on structure and physical properties. Solid State Sci. **12**(5), 699–705 (2010)
55. B. Atilla, I. Ergin, M. Gürsul, B. Özçelik, M.A. Madre, A. Sotelo, Impact of silver addition on the superconducting performances of Bi2Sr2Ca0.925Na0.075Cu2Oy:Ag composite fibers. J. Eur. Ceram. Soc. **42**(14), 6551 (2022)
56. D. Yazici, M. Erdem, B. Ozcelik, Improvement of the intergranular pinning energy in the $(BiPb)_2Sr_2Ca_2Cu_3O_{10+\delta}$ superconductors doped with high valancy cations. J. Supercond. Nov. Magn. **25**, 725–729 (2012)
57. A. Aftabi, M. Mozaffari, Intergranular coupling, critical current density, and phase formation enhancement of polycrystalline $Bi_{1.6}Pb_{0.4}Sr_2Ca_2Cu_3O_{10-y}$ superconductors by α-Al2O3 nanoparticle addition. J. Supercond. Nov. Magn. **28**, 2337 (2015)
58. S.B. Guner, Y. Zalaoglu, T. Turgay, O. Ozyurt, A.T. Ulgen, M. Dogruer, G. Yildirim, A detailed research for determination of Bi/Ga partial substitution effect in Bi-2212 superconducting matrix on crucial characteristic features. J. Alloys Compd. **772**, 388 (2019)
59. M. Tinkham, *Introduction to superconductivity*, 2nd edn. (McGraw-Hill, NY, 1996)
60. D. Sharma, R. Kumar, V.P.S. Awana, Temperature and field dependence of thermally activated flux flow resistance in $Bi_2Sr_2CaCu_2O_{8+\delta}$ superconductor. Solid State Commun. **152**, 941–946 (2012)
61. M. Me.Barakat, K. Habanjar, Magnetoresistivity studies for BiPb-2223 phase added by BaSnO3 nanopart4icles. J Adv Ceram. **6**(2), 100–109 (2017)
62. M. Rupp, A. Gubta, C.C. Tsuei, Magnetic field induced broadening of the resistive transition in epitaxial c-axis-oriented HgBa2CaCu2O6+δ films. Appl. Phys. Lett. **67**, 291 (1995)
63. Nkum, W.R. Datars, Weak link in ceramic In-doped BiPb-Sr-Ca-Cu-O. Supercond. Sci. Technol **8**, 822 (1995)

64. N.H. Mohammed, A.I. Abou-Aly, R. Awad, M. Rekaby, Magnetoresistance studies of Tl-1212 phase substituted by scandium. Supercond. Sci. Technol. **19**, 1104 (2006)
65. E. Govea-Alcaide, I. García-Fornaris, P. Muné, R.D. Jardim, Improvement of the intergranular pinning energy in uniaxially compacting (Bi-Pb)2Sr2Ca2Cu3O10+δ ceramic samples. Eur. Phys. J. B. **58**, 373 (2007)
66. S. Kurnaz, B. Cakır, A. Aydiner, The effect of growth temperature on the irreversibility line of MPMG YBCO bulk with Y2O3 layer. Cryogenics **85**, 51 (2017)
67. N.R. Werthamer, E. Helfand, P.C. Hohenberg, Temperature and purity dependence of the superconducting critical field, Hc2 III. electron spin and spin-orbit effects. Phys. Rev. **147**, 295 (1966)
68. Y. Zalaoglu, G. Yildirim, H. Buyukuslu, N.K. Saritekin, A. Varilci, C. Terzioglu, O. Gorur, Important defeats on pinning of 2D pancake vortices in highly anisotropic Bi-2212 superconducting matrix with homovalent Bi/La substitution. J. Alloys Compd. **631**, 111–119 (2015)
69. B.A. Albiss, I.M. Obaidat, M. Gharaibeh, H. Ghamlouche, S.M. Obeidat, Impact of addition of magnetic nanoparticles on vortex pinning and microstructure properties of Bi–Sr Ca–Cu–O superconductor. Solid State Commun. **150**(33–34), 1542–1547 (2010)
70. C.P. Bean, J.D. Livingston, Surface barrier in type-II superconductors. Phys. Rev. Lett. **12**, 14–16 (1964)
71. S. Vinu, P.M. Sarun, R. Shabna, A. Biju, U, Syamaprasad, Enhancement of flu5x pinning and Anderson–Dew-Hughes pinning analysis in $Bi_{1.6}Pb_{0.5}Sr_{2-x}Tb_xCa_{1.1}Cu_{2.1}O_{8+\delta}$ superconductor, J. Alloys. Compd. **477**(1–2) (2009)
72. E.J. Kramer, Scaling laws for flux pinning in hard superconductors. J. Appl. Phys. **44**(3), 1360–1370 (1973)
73. M. Li, L. Chen, W.L. You, J. Ge, J. Zhang, Giant increase of critical current density and vortex pinning in Mn doped KxFe2- ySe2 single crystals. Appl. Phys. Lett. (2014). https://doi.org/10.1063/1.4901902
74. M.S. Shalaby, M.H. Hamed, N.M. Yousif, H.M. Hashem, The impact of the addition of Bi2Te3 nanoparticles on the structural and the magnetic properties of the Bi-2223 high-Tc superconductor. Ceram. Int. **47**(18), 25236–25248 (2021)
75. D. Sharma, R. Kumar, V.P.S. Awana, DC and AC susceptibility study of sol–gel synthesized Bi2Sr2CaCu2O8+δ superconductor. Ceram. Int. **39**(2), 1143–1152 (2013)
76. D. Dew-Hughes, Flux pinning mechanisms in type II superconductors. Philos. Mag. **30**(2), 293–305 (1974)

Publisher's Note Springer Nature remains neutral with regard to jurisdictional claims in published maps and institutional affiliations.